Targeted Crystal Growth of Uranium Gallophosphates Via the Systematic Exploration of the UF4-GaPO4-ACl (A = Cs, Rb) Phase Space

Journal:	*CrystEngComm*
Manuscript ID	CE-ART-03-2020-000343.R1
Article Type:	Paper
Date Submitted by the Author:	02-Apr-2020
Complete List of Authors:	Juillerat, Christian; University of South Carolina, Department of Chemistry and Biochemistry Klepov, Vladislav; University of South Carolina, Department of Chemistry and Biochemistry Smith, Mark; University of South Carolina, Department of Chemistry and Biochemistry Zur Loye, Hans-Conrad; University of South Carolina, Department of Chemistry and Biochemistry

Targeted Crystal Growth of Uranium Gallophosphates Via the Systematic Exploration of the UF$_4$-GaPO$_4$-ACl (A = Cs, Rb) Phase Space

Christian A. Juillerat,[†§] Vladislav V. Klepov,[†] Mark D. Smith,[†] Hans-Conrad zur Loye*[†§]

[†]Department of Chemistry and Biochemistry, University of South Carolina, Columbia, SC, 29208, United States

[§]Center for Hierarchical Wasteform Materials (CHWM), University of South Carolina, Columbia, SC, 29208, United States

Abstract. The molten flux synthesis of a uranium gallophosphate and a uranium gallate, Cs$_4$[(UO$_2$(GaP$_2$O$_8$)$_2$] (**1**) and Cs$_2$UO$_2$Ga$_2$O$_5$ (**2**), and four uranium phosphates, [Rb$_2$Rb$_{3.93}$Cl$_{0.93}$][(UO$_2$)$_5$(PO$_4$)$_5$] (**3**), Rb$_{11}$[(UO$_2$)$_8$(PO$_4$)$_9$] (**4**), Rb$_{7.6}$[(UO$_2$)$_8$O$_{8.6}$F$_{0.4}$(PO$_4$)$_2$] (**5**), and Rb$_6$[(UO$_2$)$_5$O$_2$(PO$_4$)$_4$] (**6**) is reported. A systematic exploration of the UF$_4$-GaPO$_4$-ACl (A = Cs, Rb) phase space resulted in the synthesis of targeted Cs$_4$[(UO$_2$(GaP$_2$O$_8$)$_2$] (**1**) and Cs$_2$UO$_2$Ga$_2$O$_5$ (**2**), which are gallium analogs to the previously reported aluminates, Cs$_4$[(UO$_2$(AlP$_2$O$_8$)$_2$] and Cs$_2$UO$_2$Al$_2$O$_5$ (**2**). The exploration of this phase space simultaneously led to the synthesis and characterization of four new uranium phosphate phases. Rb$_2$Rb$_{3.93}$Cl$_{0.93}$][(UO$_2$)$_5$(PO$_4$)$_5$] (**3**), a salt inclusion material, and Rb$_{11}$[(UO$_2$)$_8$(PO$_4$)$_9$] (**4**) both of which have complex 3D, porous, framework structures, and Rb$_{7.6}$[(UO$_2$)$_8$O$_{8.6}$F$_{0.4}$(PO$_4$)$_2$] (**5**) and Rb$_6$[(UO$_2$)$_5$O$_2$(PO$_4$)$_4$] (**6**) both of which are layered structures related to the U$_3$O$_8$ topology. Fluorescence spectroscopy data is reported for all compositions and is found to be typical for uranyl compounds.

Introduction. According to the periodic law, the elements in the same groups have similar properties and reactivities and, consequently, can be found to form analogous compounds. Specifically, in solid state chemistry, there are several well-known pairs of main group elements that form many analogous compounds, such as Si and Ge, P and As, and Al and Ga. Some well-known structure types that accommodate these pairs interchangeably are Si and Ge wadeites,[1–6] P and As apatites,[7–9] and Al and Ga corundum structures.[10] Among these pairs, Al and Ga are most similar in size with tetrahedra crystal radii of 0.53 and 0.61 Å when compared to Si and Ge, whose tetrahedral crystal radii are 0.40 and 0.53 Å, to P and As, whose tetrahedral crystal radii are 0.31 and 0.475 Å. In addition, both Al and Ga adopt trigonal pyramidal and octahedral coordination environments with crystal radii of 0.62 and 0.69 Å, and 0.675 and 0.76 Å for each element and coordination geometry, respectively, and are thus significantly closer in size to each other than are other main group element pairs.[11] Due to the chemical similarity of these elements, once a compound containing one of them has been synthesized, one can expect that the analog will adopt the same structure, which, however, is not always the case, and sometimes even a subtle size change (and respective change in the lattice energy) can result in a completely different structure.[12] The structure types that are sensitive to the size changes can even be used for element separations,[13] fostering studies on isostructural series.

Recently, our group has published several uranium and aluminum containing oxides with complex, unique structure types and because of the similarity of Al and Ga in oxide structures,[14, 15] in addition to the lack of uranium and gallium containing phases (only two reported in the ICSD),[16] we sought to prepare the Ga analogs of these aluminum based structures. In order to target these Ga analogs, we used the same synthetic approach as was

used for the aluminum phases and systematically explored the phase space in close proximity to the successful conditions for the Al containing phases. The Al structures were synthesized via molten flux crystal growth methods[17, 18] and, as in most synthetic techniques, there is a continuum of experimental conditions that control and influence the products obtained in addition to their quality and yield. In this study, we identified the crucible size/shape, crucible material, UF_4/$GaPO_4$ reagent ratio, amount of flux, identity of the flux, and dwell temperature, and found them all strongly to influence the formation the desired products. There are a number of other variables such as dwell time, slow cooling rate, atmosphere, uranium source, gallium source, etc., that were also considered.

Not unexpectedly, in the process of exploring the UF_4-$GaPO_4$-ACl (A = Cs, Rb) phase space, we came across several new structure types in addition to two of the desired uranium and gallium containing phases we targeted. We explored a significant fraction of the phase space targeting the desired phases, and while these experiments certainly are not exhaustive and leave several variables to be explored further, they embody a representative cross section of phase space. Herein, we present the two uranium-gallium analogs, $Cs_4[(UO_2(GaP_2O_8)_2]$ (**1**) and $Cs_2UO_2Ga_2O_5$ (**2**), in addition to the compilation of uranium phosphate structures obtained in the same phase space: $[Rb_2Rb_{3.93}Cl_{0.93}][(UO_2)_5(PO_4)_5]$ (**3**), $Rb_{11}[(UO_2)_8(PO_4)_9]$ (**4**), $Rb_{7.6}[(UO_2)_8O_{8.6}F_{0.4}(PO_4)_2]$ (**5**), and $Rb_6[(UO_2)_5O_2(PO_4)_4]$ (**6**).

Experimental

Synthesis. For the synthesis of all of the reported structures, molten flux methods using alkali chloride or alkali fluoride fluxes were used.[17, 18] UF_4 (International Bio-Analytical Industries, powder, ACS grade), $UO_2(CH_3CO_2)_2 \cdot 2H_2O$ (International Bio-

Analytical Industries, powder, ACS grade), $(NH_4)_2HPO_4$ (VWR, ACS grade), CsCl (VWR, ultra pure), CsF (Alfa Aesar, 99%), RbCl (BTC, 99.0%) were all used as received. $GaPO_4$ is not available commercially and was therefore synthesized by us using a 1:2 mol mixture of Ga_2O_3 (Alfa Aesar, 99.999%) and $(NH_4)_2HPO_4$ that was intimately ground in a mortar and pestle before heating the mixture at 1000 °C for 40 hours. The resulting $GaPO_4$ was determined to be a mixture of two polymorphs and contained a small Ga_2O_3 impurity and was used, as is, in the following reactions. ***Caution!*** *Although the uranium precursors used* *contained depleted uranium, standard safety measures for handling radioactive substances* *must be followed.*

$Cs_4[(UO_2(GaP_2O_8)_2]$ (**1**). Synthesis methods are based on those used to synthesize $Cs_4[(UO_2(AlP_2O_8)_2].$[14] Single crystals of **1** were obtained by reacting 0.5 mmol of UF_4, 1 mmol $GaPO_4$, 1 mmol $(NH_4)_2HPO_4$, and 20 mmol CsCl in a 17 mL Pt crucible, open to atmosphere, (28.5 mm ID x 27 mm tall) and heating the mixture at 700 °C for 12 h and slow cooling to 600 °C at 6 °C/h. Crystals were isolated from the reaction by sonicating the reaction in water to dissolve the flux, followed by vacuum filtration—the same method is used for all syntheses reported. Small, pale yellow needle shaped crystals (Figure 1) were obtained in good yield alongside other minor impurity phases. Solid state reactions were also carried out by intimately grinding 1 mmol of $UO_2(CH_3CO_2)_2 \cdot 2H_2O$, 2mmol $GaPO_4$, 2 mmol $(NH_4)_2HPO_4$, and 4 mmol of $CsNO_3$ and pressing a pellet and heating at 575 °C for 66 h, and 700, 800, and 900 °C for 12 h. In between changes in temperature, the pellets were intermittently ground and pressed into pellets before heating at a high temperature. While $Cs_4[(UO_2Ga_2(PO_4)_4]$ (**1**) was obtained, the simultaneous formation of a significant

quantify of an impurity phase could not be avoided; unfortunately, this impurity phase could not be identified (Figure 2).

$Cs_2UO_2Ga_2O_5$ (**2**). Yellow, kite-shaped single crystals of **2** were grown by loading 0.5 mmol UF_4, 0.5 mmol Ga_2O_3, 11 mmol of CsCl, and 9 mmol of CsF in a 17 mL Pt crucible (28.5 mm ID x 27 mm tall) and heating at 875 °C for 12h before slow cooling to 450 °C at 6 °C/h. $Cs_4U_5O_{17}$ was simultaneously obtained as orange rods that grew on the walls of the crucibles, while the yellow crystals of **2** were found at the bottom of the crucible.
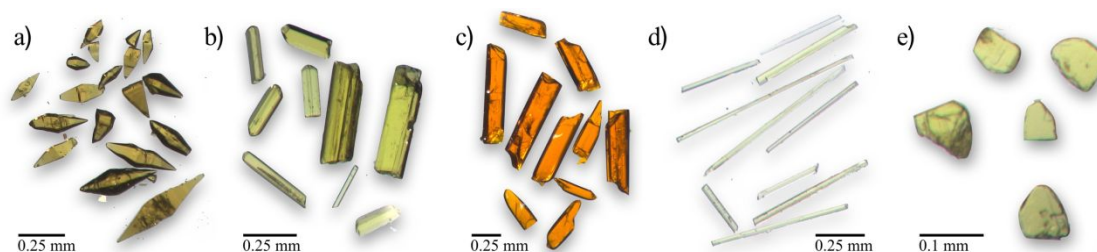

Figure 1: Optical images of single crystals of a) $Cs_2UO_2Ga_2O_5$ (**2**) b) $[Rb_2Rb_{3.93}Cl_{0.93}][(UO_2)_5(PO_4)_5]$ (**3**) c) $Rb_{7.6}[(UO_2)_8O_{8.6}F_{0.4}(PO_4)_2]$ (**5**), d) $Rb_{11}[(UO_2)_8(PO_4)_9]$ (**4**), and e) $Rb_6[(UO_2)_5O_2(PO_4)_4]$ (**6**).

Crystals of $[Rb_2Rb_{3.93}Cl_{0.93}][(UO_2)_5(PO_4)_5]$ (**3**) and $Rb_6[(UO_2)_5O_2(PO_4)_4]$ (**6**) were obtained by loading 0.5 mmol UF_4, 0.5 mmol $GaPO_4$, and 20 mmol RbCl in an open fused silica tube (14 mm ID x ~26 mm tall) and covered with a silica cap (17 mm ID x ~20 mm tall). The reactions were heated to 875 °C and held there for 12 h before slow cooling to 550 °C at 6 °C/h. Both **3** and **6** are yellow crystals, where **3** is the more predominant product that crystallizes as rods/needles, while **6** crystallizes as plates.

$Rb_{11}[(UO_2)_8(PO_4)_9]$ (**4**) was obtained from a reaction of 0.5 mmol of UF_4, 1 mmol $GaPO_4$, and 20 mmol of RbCl loaded into a 5 mL Pt crucible (15 mm ID x 26 mm tall) and heated at 875 °C for 12 h before slow cooling to 550 °C at 6 °C/h. The single crystals are

pale-yellow in color and are long needles, a side product that is deeper yellow in color as well as more rod like was also obtained and was identified as $Rb_9U_5P_6O_{34.5}$; however, the crystal quality was very poor and the SXRD structure cannot be reported with confidence.

Single crystals of $Rb_{7.6}[(UO_2)_8O_{8.6}F_{0.4}(PO_4)_2]$ (**5**) were obtained in a reaction of 0.5 mmol UF_4, 0.33 mmol of $GaPO_4$, and 20 mmol of RbCl in a 5 mL alumina crucible (16 mm ID x 26 mm tall) with a larger 17 mL alumina crucible (23.5 mm ID x 41.5 mm tall) inverted overtop. The reaction was heated at 775 °C for 12 h and slow cooled to 650 °C at 6 °C/h. This synthesis produced a least 5 different phases either yellow or orange in color and varying in crystal morphology. $Rb_6[(UO_2)_5O_5(PO_4)_2]$, $Rb_7[Al_2O(PO_4)_3][(UO_2)_6O_4(PO_4)_2]$, $Rb_3[Al_2O(PO_4)_3][(UO_2)_3O_2]$, were among those identified. Crystals of **5** form as orange rectangular prisms (Figure 1).

PXRD. A Bruker D2 Phaser equipped with a LYNXEYE silicon strip detector with a Cu Kα (λ = 1.54056 Å) source was used to collect PXRD data. PXRD patterns were used for product identification.

Single Crystal X-ray Diffraction. Except for **1**, the structures of each of the reported compounds were determined by single crystal X-ray diffraction (SXRD) using data collected on a Bruker D8 QUEST diffractometer with an PHOTON II area detector and a microfocus source (Mo Kα radiation, λ = 0.71073 Å) or a Bruker D8 QUEST diffractometer equipped with a PHOTON 100 CMOS area detector and a microfocus source (Mo Kα radiation, λ = 0.71073 Å). The raw data were reduced and corrected for absorption effects using SAINT+ and SADABS programs within APEX 3.[19] The SHELXT solution program employing intrinsic phasing was used to obtain an initial structure that was refined using the SHELXL refinement program.[20] Both SHELXT and SHELXL were

Table 1: Full crystallographic data for compounds **1-6**.

Formula	$Cs_4[(UO_2Ga_2(PO_4)_4]$	$Cs_2UO_2Ga_2O_5$	$[Rb_{5.93}Cl_{0.93}][(UO_2)_5(PO_4)_5]$	$Rb_{11}[(UO_2)_8(PO_4)_9]$	$Rb_{7.6}[(UO_2)_8O_{8.6}F_{0.4}(PO_4)_2]$	$Rb_6[(UO_2)_5O_2(PO_4)_4]$
Number	**1**	**2**	**3**	**4**	**5**	**6**
S. G.	--	$I4/amd$	$P\bar{1}$	$P4_2/mbc$	$P2_1/n$	$P\bar{1}$
a, Å	10.837(1)	7.41690(10)	9.548(4)	25.7697(6)	9.5935(5)	7.3052(8)
b. Å	10.857(1)	7.41690(10)	13.488(5)	25.7697(6)	13.7652(8)	9.0828(10)
c, Å	13.018(1)	31.9700(7)	14.898(6)	9.3962(2)	13.2983(8)	11.7254(13)
α, °	80.564(4)	90	64.755(16)	90	90	75.857(4)
β, °	82.786(4)	90	72.369(16)	90	101.343(2)	72.834(4)
γ, °	87.026(4)	90	89.511(16)	90	90	86.974(4)
V, Å³	1498.1(2)	1758.68(6)	1637.7(11)	6239.8(3)	1721.82(17)	720.65(14)
Crystal size (mm³)	--	0.02 x 0.04 x 0.06	0.02 x 0.03 x 0.04	0.02 x 0.02 x 0.1	0.01 x 0.02 x 0.03	0.04 x 0.12 0.16
temp. (K)	--	302	301	301	303	301
density (g cm⁻³)	--	5.708	4.796	4.212	6.066	5.242
θ range (deg)	--	2.548–36.353	2.260–28.437	2.499–27.500	2.151–27.492	2.313–37.883
μ (mm⁻¹)	--	32.620	33.813	29.564	48.351	38.389
collected reflec.	--	61580	74700	100392	109936	52660
unique reflections	--	1204	8125	3807	3952	7778
R_{int}	--	0.0352	0.0882	0.0452	0.0674	0.0499
h	--	$-12 \leq h \leq 12$	$-12 \leq h \leq 12$	$-33 \leq h \leq 33$	$-12 \leq h \leq 12$	$-12 \leq h \leq 12$
k	--	$-12 \leq k \leq 11$	$-18 \leq k \leq 16$	$-33 \leq k \leq 32$	$-17 \leq k \leq 17$	$-15 \leq k \leq 15$
l	--	$-53 \leq l \leq 53$	$-19 \leq l \leq 19$	$-12 \leq l \leq 12$	$-17 \leq l \leq 17$	$-20 \leq l \leq 20$
$\Delta\rho_{max}$ (e Å⁻³)	--	1.481	2.772	2.126	2.573	2.800
$\Delta\rho_{min}$ (e Å⁻³)	--	-1.450	-3.161	-1.686	-2.114	-2.897
GoF	--	1.326	1.098	1.326	1.362	1.056
$R_1(F)$ for $F_0{}^2>2\sigma (F_0{}^2)^a$	--	0.0210	0.0482	0.0350	0.0405	0.0282
$R_w(F_0{}^2)^b$	--	0.0498	0.0960	0.0910	0.0865	0.0728

$^aR_1 = \Sigma||F_0| - |F_c||/\Sigma|F_0|$. $^bwR_2 = \left[\Sigma w\left(F_0{}^2 - F_c{}^2\right)^2/\Sigma w\left(F_0{}^2\right)^2\right]^{1/2}$

used within the Olex2 GUI.[21, 22] Full crystallographic details can be found in Table 1. Elemental compositions of the compounds were confirmed qualitatively by EDS using a TESCAN Vega-3 SBU equipped with an EDS detector.

Attempts were made to collect high quality SXRD data on compound **1**; however, due to multiple twinning and generally insufficient crystal quality, a publishable structure solution could not be obtained. The unit cell data obtained from single crystals is reported in Table 1 and the PXRD pattern of the product obtained by solid state synthesis with calculated pattern using the cif of $Cs_4[(UO_2(AlP_2O_8)_2]$ and changing the unit cell contents from Al to Ga and unit cell parameters produces a nice fit (Figure 2) and confirms that the Ga analog has been obtained.

For $Cs_2UO_2Ga_2O_5$ (**2**), the refinement of the U, Ga, and O sites was straightforward, while the refinement of the Cs sites was difficult due to the extreme disorder of the cations in the channels of the structures, similar to what was observed in the Al analog. Partially occupied Cs sites were added by freely refining significant electron density peaks near the largest Cs sites, Cs1 and Cs2, until the summed occupancies of these sites approached charge balance, 2 Cs per formula unit. At this point the occupancies of the sites were fixed, refined anisotropically, and an ISOR command was implemented on Cs2 to restrain the thermal parameters on the Cs sites, and then the occupancies of individual sites were manually and slowly increased to achieve charge balance. This was done manually instead of using a constraint such as the SUMP command, due to the instability of the refinement when this constraint is applied. The final occupancies of Cs1-Cs7 are 0.6338, 0.13, 0.0445, 0.052, 0.0408, 0.10, and 0.05, respectively.

For $[Rb_2Rb_{3.93}Cl_{0.93}][(UO_2)_5(PO_4)_5]$ (**3**), difficulty was encountered in finding a crystal of suitable diffraction quality for structure determination. Several crystals and cleaved crystal fragments were screened for quality and most exhibited problematic, twinned diffraction patterns consisting of very closely run-together spots, also having poorly shaped, asymmetric Bragg peak profiles with long tails. Three datasets were collected on small cleaved fragments, and the best is reported here. The compound crystallizes in the triclinic system. The space group $P\overline{1}$ (No. 2) was confirmed by structure solution. The asymmetric unit consists of five uranium atoms, six rubidium atoms, five phosphorus atoms, one chloride atom, one mixed and partially occupied Rb/Cl site and thirty unique oxygen atoms. All atoms are located on positions of general crystallographic symmetry (site $2b$). Several displayed poorly shaped displacement ellipsoids arising from the moderate crystallinity or from crystallographic disorder.

Uranium atoms U1-U4 refine normally. U5 is disordered over three closely separated sites. Refinement of the U5 site as a single position resulted in an elongated displacement ellipsoid, two large satellite electron density peaks (9.4 and 3.2 e-/$Å^3$) at *ca.* 0.8 Å from the position, and an R_1 value > 9%. A disordered, 3-part U5 site better accounted for the observed electron density and reduced the R_1 value to 4.82%. The three components were restrained to sum to one uranium per site and refined to U5(A/B/C) = 0.730(3)/0.190(3)/0.080(3). This results in distorted coordination environments for U5B and U5C (Figure 5e) and very short and long equatorial bond distances. It is possible that the O atoms coordinated to these U sites are also disordered to create more reasonable coordination environments, but due to the small scattering factors and low occupancy of the O, this disorder could not be modeled. The uranyl oxygen, however, was able to be

modeled as a split site. Oxygen O28, as a U5 uranyl unit oxygen atom, is disordered over two sites A/B. Occupancies of the two sites were tied to the U5A (O28A) and U5(B/C) (O28B) occupancies, thereby corresponding to two typical, nearly linear UO_2 groups (with O29).

Disorder or partial occupancy was also observed for rubidium sites Rb3 - Rb6. Only Rb1 and Rb2 refined to full occupancy and without the appearance of large nearby residual density. Rb3 and Rb4 are each disordered over two sites with occupancies Rb3(A/B) = 0.69(8)/0.31(8) and Rb4A/B = 0.65(2)/0.35(2) (both constrained to sum to one). Rb5 refines to a partial occupancy value of 0.844(7). There were no residual peaks close to Rb5 suggesting a split site. Rb6 was modeled with three independent sites distributed roughly linearly, with occupancies Rb6(A/B/C) = 0.770(3)/0.111(3)/0.119(3). The unique chlorine atom Cl1 is disordered across an inversion center and was refined as half-occupied. Another site near the Rb6 disorder assembly was modeled as a mixed and split Rb/Cl site, Rb7A/Cl2A. This site refined to a partial occupancy value significantly less than one even if modeled as 100% Cl and was further split into two discrete electron density maxima. Several disorder models for this site were refined, but only the reported model resulted in an essentially electroneutral composition. Distances to surrounding atoms are reasonable for both Rb and Cl. Occupancies refined to Rb7A = 0.082(6) and Cl2A = 0.45(2). The U_{ij} values of oxygen O16 were restrained to adopt a spherical shape to prevent an oblate ellipsoid. All atoms were refined with anisotropic displacement parameters except for minor disorder components B and C of site Rb6 and the Rb7A/Cl2A site (isotropic).

The structure solution of $Rb_{11}[(UO_2)_8(PO_4)_9]$ (**4**) is highly disordered and the structural significance of the disorder will be discussed in the structure description section,

vide infra, while the crystallographic approach to modeling the disorder is discussed in this section. $Rb_{11}[(UO_2)_8(PO_4)_9]$ (**4**) crystallizes in the tetragonal space group $P4_2/mbc$ and the asymmetric unit contains four uranium atoms, six rubidium atoms, three phosphorus atoms, and 17 unique oxygen atoms. A large number of sites, namely U1-3, Rb1, Rb3, Rb4B, Rb6, O1. O2. O7, O13, and O14 lie on Wyckoff site 8*h* with ..*m* symmetry, Rb2, Rb5A, Rb5c lie on Wyckoff site 8*g* with ..2 symmetry, P1 is assigned to Wyckoff site 4*d* with 2.22 symmetry, and all other sites lie on general positions.

U4, along with its uranyl oxygens O17 and O18, are disordered across a mirror plane and were assigned an occupancy of 0.5. The equatorial oxygens bonded to U4, O4A/B and O5A/B are also disordered over two positions each and were assigned occupancies of 0.5 to match the U4 disorder. P3A/P3B are coordinated to O4A/B and O5/B such that the phosphate tetrahedron has two possible orientations, each half occupied to match the U4 disorder, and are coordinated to O6A/B and O3. The disorder of the P2A/B, coordinates to oxygens O9-O12, sites also represent two possible orientations for the phosphate tetrahedron (A and B) which were allowed to freely refine while constrained to a summed occupancy of 1 and result in 0.51/0.49 for part A and B, respectively. P1, coordinated to O15A/B, is also disordered over two orientations with occupancies of 0.5.

Additionally, the Rb cations are heavily disordered where there are three positions for Rb4 and four for Rb5 and Rb1-3 and Rb6 are fully occupied. Rb4A/B represents a disordered, half occupied Rb site where Rb4A is disordered over a mirror plane and the three resulting positions were constrained to a sum of 0.5 using a SUMP command resulting in occupancies of 0.2166 and 0.067, respectively for Rb4A and Rb4B. Similarly, a SUMP command was used for Rb5A/B/C (occupancies 0.475/0.1763/0.172) where Rb5B

is disordered over a two-fold rotation axis and the Rb5 sites are constrained to an occupancy of 1. All atoms were refined anisotropically, although ISOR commands were used to constrain the thermal ellipsoids of Rb4A/B, O9A, O11A, and O12A.

Rb$_{7.6}$[(UO$_2$)$_8$O$_{8.6}$F$_{0.4}$(PO$_4$)$_2$] (**5**) crystallizes in the monoclinic space group $P2_1/c$ and the asymmetric unit contains four uranium atoms, five rubidium atoms, one phosphorus atom, and 17 oxygen atoms. All atoms are located in positions of general crystallographic symmetry (4*e*) except for Rb1, which is located on an inversion center with Wyckoff site label 2*a*. Rb1 and 2 are fully occupied, while Rb3 and Rb4 are disordered and Rb5 is partially occupied. Rb3A/B and Rb4A/B were constrained to sum to an occupancy of one and refine to 0.79/0.21 and 0.66/0.34, respectively. Rb5 when freely refined resulted in a partial occupancy of 0.30. With this partially occupied Rb site, the structure formula does not charge balance if all anion sites are modeled as oxygen; however, the O4 site freely refined to an occupancy of ~1.15 suggesting that it is a shared site of oxygen and fluorine. Since the scattering factors of O and F are very similar, they are often difficult to distinguish based on X-ray diffraction data so the O4/F4 occupancies were set to 0.80/0.20 to achieve charge balance. There is minor disorder in the uranium sheets, where O11 is disordered over an inversion center and set to an occupancy of 0.5. U4A/B, coordinated to O11, is disordered over two sites, and the occupancies were set to 0.5 which maintains regular coordination environments for the U4A/B where U4A adopts a square bipyramidal coordination and U4B adopts a pentagonal coordination environment. The disorder is further discussed in the structure description section. All atoms were refined anisotropically.

The refinement of $Rb_6[(UO_2)_5O_2(PO_4)_4]$ (**6**) was straightforward and the compound crystallizes in the triclinic space group $P\bar{1}$ (No. 2) and was confirmed by structure solution. The asymmetric unit consists of three uranium atoms, three rubidium atoms, two P atoms and 14 unique oxygen atoms. All atoms are all located on positions of general crystallographic symmetry (site $2i$), except for U3, which is located on an inversion center (site $1d$). All atoms were refined with anisotropic displacement parameters.

Optical Spectroscopy. Fluorescence emission spectra (400-650 nm) were collected for single crystals of **1-6** using a free space coupled 375 nm laser and Horiba iHr320 spectrometer equipped Olympus BX53 microscope.

Results and Discussion

Synthesis. The recent success of obtaining uranium aluminophosphates and uranium aluminates by molten flux methods prompted a more expansive exploration of the UF_4, $GaPO_4$, and ACl (A = Rb, Cs) phase space with the goal of obtaining Ga analogs of the recently obtained Al containing structures: $Cs_2UO_2Al_2O_5$, $Cs_4[(UO_2Al_2(PO_4)_4]$, $[Cs_{13}Cl_5][(UO_2)_3Al_2O(PO_4)_6]$, $A_3[Al_2O(PO_4)_3][(UO_2)_3O_2]$ (A = Cs, Rb), and $Rb_7[Al_2O(PO_4)_3][(UO_2)_6O_4(PO_4)_2]$.[14, 15] While several of these compositions could be obtained using uranyl nitrate (U^{6+}) because the U^{4+} (from UF_4) readily oxidizes in oxygen-rich atmosphere at high temperatures to U^{6+}, which is found in all compositions, the use of UF_4 produced larger crystals of higher quality; therefore, we have continued to use UF_4. In several publications by Juillerat et al. the crucible size and shape was found to be essential in obtaining certain products.[23–26] In order to specifically target the Ga analogs of the

recently published U and aluminum containing materials, reaction vessels of the same size were used as in the Al synthesis.

Initially, reactions were performed in 5 mL alumina vessels, which were used in the synthesis of the Al structures, as in the reported synthesis of **5**; however, the chloride flux dissolved small amounts of the alumina crucible (no visible damage) and led to Al containing products. In order to avoid alumina incorporation, reaction vessels of the same size but different material were sought out. Fused silica reaction vessels were made from tubing to match the size of the alumina crucible and lead to the formation of **3** and **6** and reactions in this phase space are summarized in Figure S1. It was verified that the reactions reported for the synthesis of $Rb_3[Al_2O(PO_4)_3][(UO_2)_3O_2]$ could be successfully carried out in the fused silica tubes. To further study the impact of crucible size and crucible material, 5 mL Pt crucibles were used in this study. $Rb_3[Al_2O(PO_4)_3][(UO_2)_3O_2]$ could also be obtained in the 5 mL Pt vessels. The use of these crucibles led to the synthesis of **4** and **5**. The phase space of the RbCl and CsCl fluxes in Pt crucibles is summarized in Figures S2 and S3.[25, 27, 28] Interestingly, using the same reactant loading for the synthesis of **3** and **6** $UF_4/GaPO_4$ 1:1, but using Pt crucibles, led to a different product, $Rb_9U_5P_6O_{34.5}$, the complete structure of which cannot be reported due to insufficient crystal quality. However, **6** could be obtained in the 5 mL Pt crucibles at 775 °C and a 1.5:1 ratio of $UF_4/GaPO_4$. It seems that although Pt and Si did not participate in the reaction, the material of the crucible, in addition to the size/shape, played a role in the synthesis, possibly due to the difference in nucleation sites in the crucibles of different materials.

$Cs_4[(UO_2Ga_2(PO_4)_4]$ (**1**) can also be synthesized using $UO_2(CH_3CO_2)_2 \cdot 2H_2O$ (instead of UF_4), similar to the synthesis of the Al analog,[14] and using only $GaPO_4$ for the

Ga and phosphate source. Additionally, **1** can be synthesized in the smaller 5 mL Pt crucibles at 775 °C and 875 °C at a ratio of 1:2 $UF_4:GaPO_4$. At lower ratios, $Cs_2(UO_2)_2(PO_4)_2$,[29] $[Cs_4Cs_4Cl][(UO_2)_4(PO_4)_5]$,[14] or $Cs_6[(UO_2)_7O_4(PO_4)_4]$ [30] are obtained.

In the publication reporting $Cs_2UO_2Al_2O_5$,[15] crystals were obtained serendipitously; however, attempts to reproduce crystal growth were unsuccessful. In this work, we report the flux synthesis of $Cs_2UO_2Ga_2O_5$ using UF_4, Ga_2O_3, and CsCl flux in 17 mL Pt crucibles. Since the synthesis was successful for the gallium analog, adapting the same crystal growth conditions, specifically using 17 mL Pt crucibles, but substituting Al_2O_3 for Ga_2O_3, we were able to reproducibly grow crystals of $Cs_2UO_2Al_2O_5$; crystal quality, however, was poor. The original publication reporting $Cs_2UO_2Al_2O_5$, described the many variables that were changed in attempts to obtain crystals; however, the size of the reaction vessel was not one of them. Interestingly, it appears that the size of the reaction vessel is an essential variable that was overlooked in previous studies. Additionally, it was reported that $Cs_2UO_2Al_2O_5$ could not be obtained using silver tubes, and similarly, $Cs_2UO_2Ga_2O_5$ could not be obtained in silver tubes either.

Structure. $Cs_4[(UO_2Ga_2(PO_4)_4]$ (**1**) and $Cs_2UO_2Ga_2O_5$ (**2**) are analogous to $Cs_4[(UO_2Al_2(PO_4)_4]$ and $Cs_2UO_2Al_2O_5$, which are discussed in an earlier publications.[14,15] The single crystals of **1** suffered from extreme twinning and low crystal quality; however, the phase could be identified by the single crystal unit cell parameters and by comparing the calculated Ga powder diffraction pattern (using the atomic coordinates of $Cs_4[(UO_2Al_2(PO_4)_4]$ and replacing Al sites with Ga and adjusting lattice parameters to match SXRD data) with measured powder diffraction data (Figure 2). The structure of **1** is shown in Figure 3 and contains uranium gallophosphate layers (Figure 3b) where

$[Ga_2(PO_4)_4]^{6-}$ layers are connected through uranyl square bipyramids and dimers of uranyl pentagonal bipyramids.
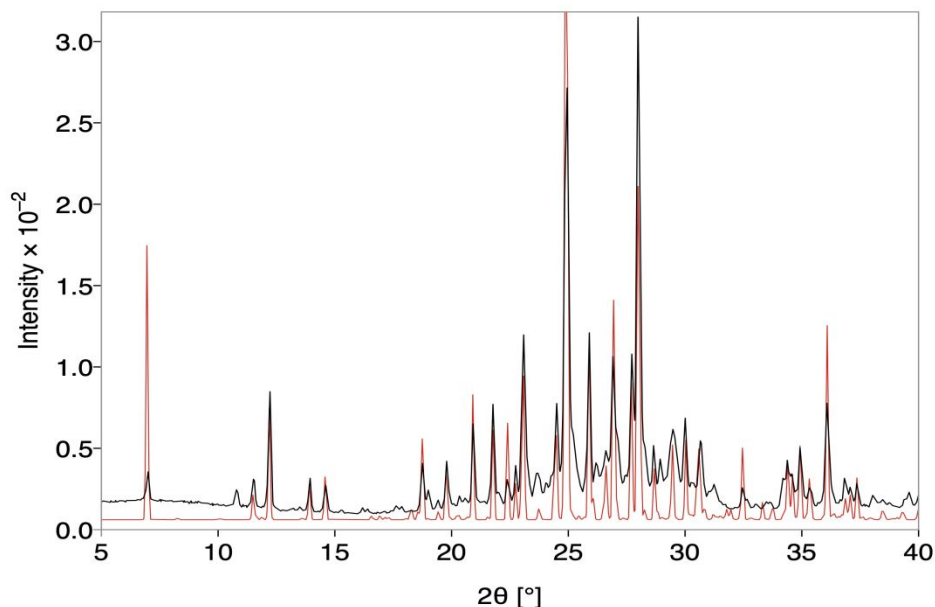

Figure 2: Powder X-ray diffraction data of **1**. The experimentally collected pattern is in black and the red is the calculated pattern from the cif of $Cs_4[(UO_2Al_2(PO_4)_4]$ with Al sites replaced with Ga and unit cell parameters from the SXRD data.

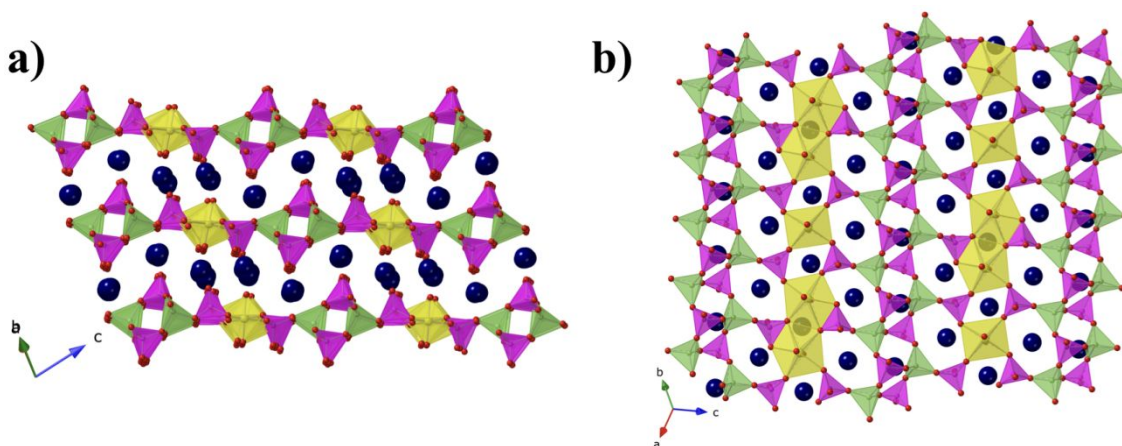**Figure 3**: The layered structure of $Cs_4[(UO_2Al_2(PO_4)_4]$. For all figures, alkali cations are blue, uranium polyhedra are yellow, phosphate tetrahedra are magenta, gallate tetrahedra are green, and oxygen atoms are red.
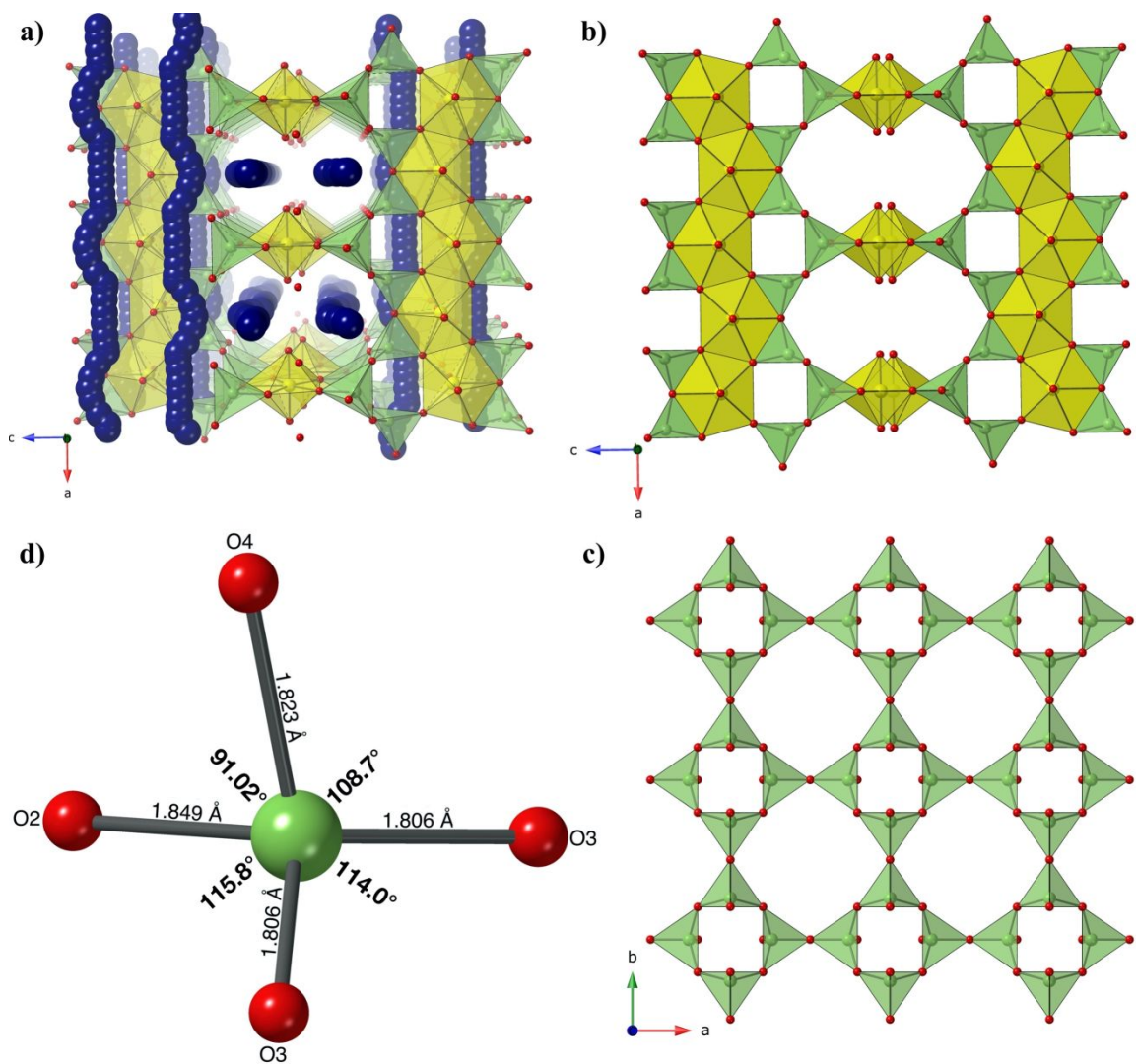
Figure 4: The structure of $Cs_2UO_2Ga_2O_5$ (**2**), a) a perspective view, b) framework with Rb cations removed, c) the 2D gallate sheets, and d) the distorted tetrahedral coordination of Ga1.

The structure of **2** is shown in Figure 4 and is constructed of 2D gallate sheets constructed of vierer and achter rings and edge sharing chains of UO_7 polyhedra. All of the gallate sheets are parallel to the *ab* plane, while the UO_7 chains alternate between the *a* and *b* directions between each gallate sheet. As expected, the Ga-O bonds are longer than the Al-O bonds in the Al analog. For comparison, the Ga-O bonds in **2** are 1.806(2), 1.8229(13), 1.849(4) Å, while the Al-O bond distances are 1.7263(16), 1.773(3), and

1.7489(13) Å (bond distances and bond valences sums for all structures are in Tables S4-8). In both structures the tetrahedra are slightly distorted with the smallest angle being 95.159° in the Al and 91.022° in the Ga structure. Between the Ga and Al analogs, there is no significant change in the equatorial U-O bond lengths with average bond lengths of 2.34 Å and 2.33 Å in the Al and Ga structures, respectively; therefore, the longer Ga-O bond lengths lead to a larger distortion in the tetrahedron. As in the Al structure, the Cs cations are heavily disordered throughout the channels created by the parallel UO_7 chains.

U, Ga, O containing structures are limited to a handful of compositions in the ICSD database, namely $Cs[(UO_2Ga(PO_4)_2]$ and $Cs_4[(UO_2)_2(GaOH_2)(PO_4)_4]•H_2O$ which were synthesized by mild hydrothermal methods.[16] Both structures are constructed of uranyl pentagonal bipyramid dimers, phosphate tetrahedra, gallate tetrahedra, and $Cs_4[(UO_2)_2(GaOH_2)(PO_4)_4]•H_2O$ additionally contains gallium octahedra.

$[Rb_2Rb_{3.93}Cl_{0.93}][(UO_2)_5(PO_4)_5]$ (**3**) is a uranyl phosphate salt inclusion material (SIM), where the salt inclusion and non-salt inclusion ions are in the first set of brackets, and the framework is in the second set of brackets. Many uranyl silicate and germanate SIMs have been recently reported,[31–35] and while there are several transition metal phosphate SIMs,[36–40] only two other uranyl phosphate SIMs have been reported thus far.[14] The framework consists of PO_4 tetrahedra, UO_6, and UO_7 polyhedra and contains two different types of channels, one channel houses the non-salt inclusion Rb cations, and the other hosts the $Rb_{3.93}Cl_{0.93}^{3+}$ salt inclusion. The structure can be broken down into uranium phosphate sheets, Figure 5c, that are connected to other sheets by the chains in Figure 5b. The $[(UO_2)_2(PO_4)_3]^{5-}$ sheets contain chains of edge sharing dimers of uranyl pentagonal bipyramids that edge share to two phosphate tetrahedra and that are connected to other

dimers through corner sharing phosphate tetrahedra. The edge sharing phosphate tetrahedra

also edge shares with a UO_2 polyhedron. These chains and additional UO_7 polyhedra create

12 membered (U-P) rings that create pores orthogonal to the channels in the *a* direction.

The $[(UO_2)_2(PO_4)_3]^{5-}$ sheets are connected to the $[(UO_2)_3(PO_4)_2]$ chains, which are the same

as those in the sheets, through the UO_6 polyhedra. The complex, disordered 1D salt

inclusion is shown in Figure 5d, and roughly consists of two isolated Cl atoms, one

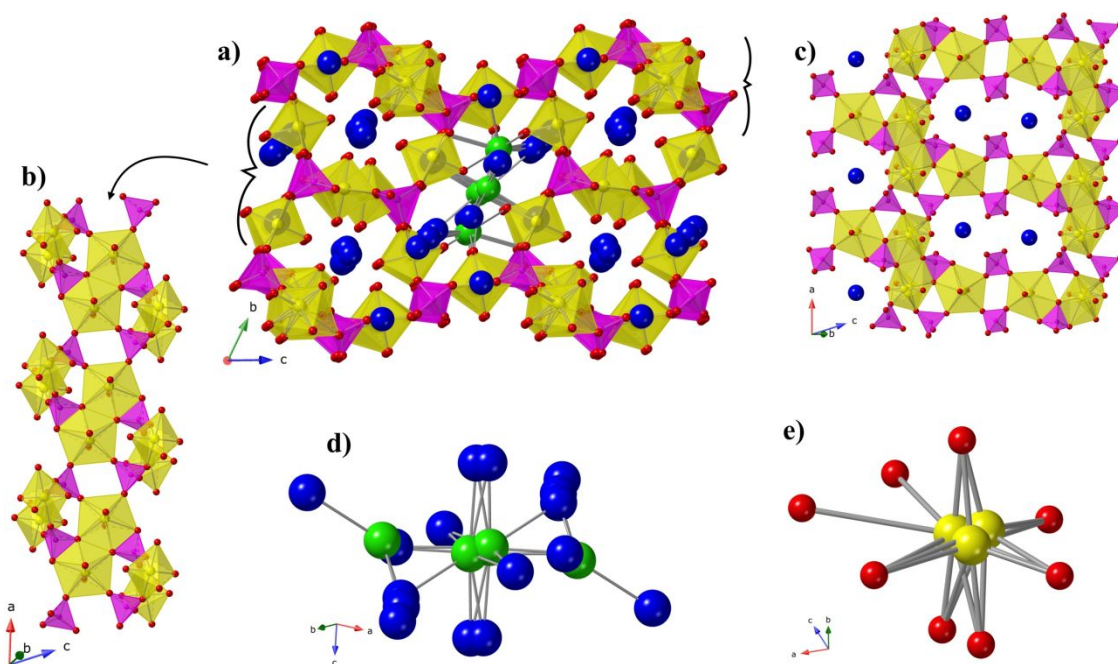coordinated to 4-7 Rb cations and the other coordinated to 4 O and 1-2 Rb.

Figure 5: The structure of $[Rb_2Rb_{3.93}Cl_{0.93}][(UO_2)_5(PO_4)_5]$ (**3**). a) the framework and all ions, b) the $[(UO_2)_3(PO_4)_2]$ chains, c) the $[(UO_2)_2(PO_4)_3]^{5-}$ sheets, d) the $[Rb_{3.93}Cl_{0.93}]^{3+}$ salt inclusion, and e) the disordered U5A/B/C site.

The structure of $Rb_{11}[(UO_2)_8(PO_4)_9]$ (**4**) is a 3D channel structure with three unique

channels and is built of phosphate tetrahedra and UO_7 pentagonal bipyramids (Figure 6).

It can be deconstructed into large channels, pinwheels, and chains. The $[(UO_2)_2(PO_4)_4]^{8-}$

channels (two per formula unit) are shown in Figure 6d and consist of pairs of uranyl

pentagonal bipyramids bridged together through edge sharing of two phosphate tetrahedra.

The edge sharing PO_4 groups connected to these UO_7 polyhedra are disordered, where the

purple and magenta colored tetrahedra represent two possible orientations. The idealized

structure would have one edge sharing phosphate per UO_7 polyhedra and all of these

tetrahedra would point in the same direction down the c axis. These $[(UO_2)_2(PO_4)_4]^{8-}$ units,

similar to those seen in the $[(UO_2)_2(PO_4)_3]^{5-}$ sheets found in **3** (Figure 6c), connect to others

that are approximately orthogonal to create the channels that house the Rb cations. These

channels are quite large with a distance of 9.442 Å between two O8 atoms across the
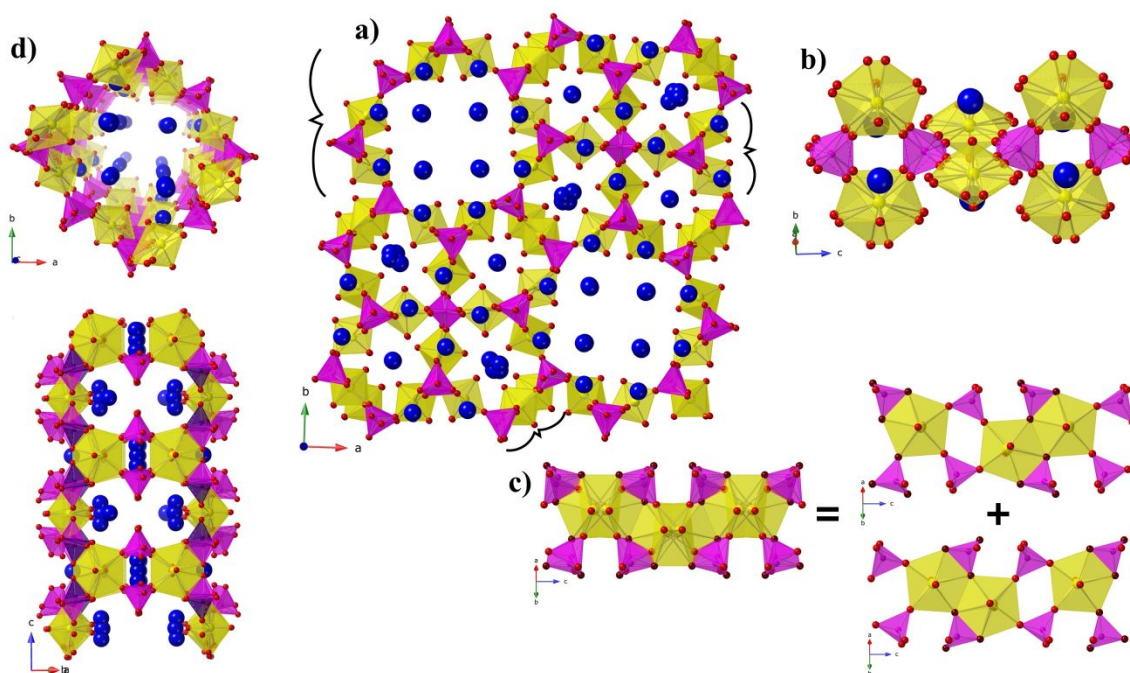
channels.

Figure 6: The structure of $Rb_{11}[(UO_2)_8(PO_4)_9]$ (**4**). a) the overall structure, b) the $[(UO_2)_2(PO_4)]^+$ pinwheels, d) the disordered chains of $(UO_2)_2^{4+}$ dimers, and d) the $[(UO_2)_2(PO_4)_4]^{8-}$ channels.

The channels are directly connected through corner sharing tetrahedra to the $[(UO_2)_2(PO_4)]^+$ pinwheels shown in Figure 6b. There are two possible orientations of the phosphate tetrahedra in this unit with two possible equatorial oxygen positions for each U atom. The last building unit for structure **4** are the $(UO_2)_2^{4+}$ dimers of uranyl pentagonal bipyramids (Figure 6c) that coordinate to phosphate tetrahedra in the $[(UO_2)_2(PO_4)_4]^{8-}$ channels. The chains created by the $(UO_2)_2^{4+}$ dimers and the phosphate tetrahedra from the $[(UO_2)_2(PO_4)_4]^{8-}$ channels are disordered over two possible orientations as shown in Figure 6c. The $(UO_2)_2^{4+}$ dimers connect diagonally adjacent $[(UO_2)_2(PO_4)_4]^{8-}$ channels and between the $(UO_2)_2^{4+}$ dimers and the pinwheels are small pores which house additional Rb cations.

Both structures $Rb_{7.6}[(UO_2)_8O_{8.6}F_{0.4}(PO_4)_2]$ (**5**) and $Rb_6[(UO_2)_5O_2(PO_4)_4]$ (**6**) are uranyl phosphate layered structures that house Rb cations between layers and are related to the U_3O_8 topologies. Building units of the α- and β-U_3O_8 topologies are shown in Figure 7e and 7f, respectively and are constructed of two chains of edge-sharing pentagonal bipyramids that mirror each other and are connected through additional edge-sharing UO_7 or UO_6 polyhedra in the α- and β- topologies, respectively. Figure 7c shows the disordered U_3O_8 based building units in **5** and Figure 7d shows the idealized unit where one of the U sites that connects the two chains is a square bipyramid and the other is a pentagonal bipyramid, which can be described as a combination of the α- and β-U_3O_8 topologies. The bridging U atom is disordered over two sites, where one corresponds to the square and the other to the pentagonal coordination environment. These U_3O_8 building units are combined into a sheet where adjacent units are rotated 90 ° and phosphate tetrahedra occupy the small

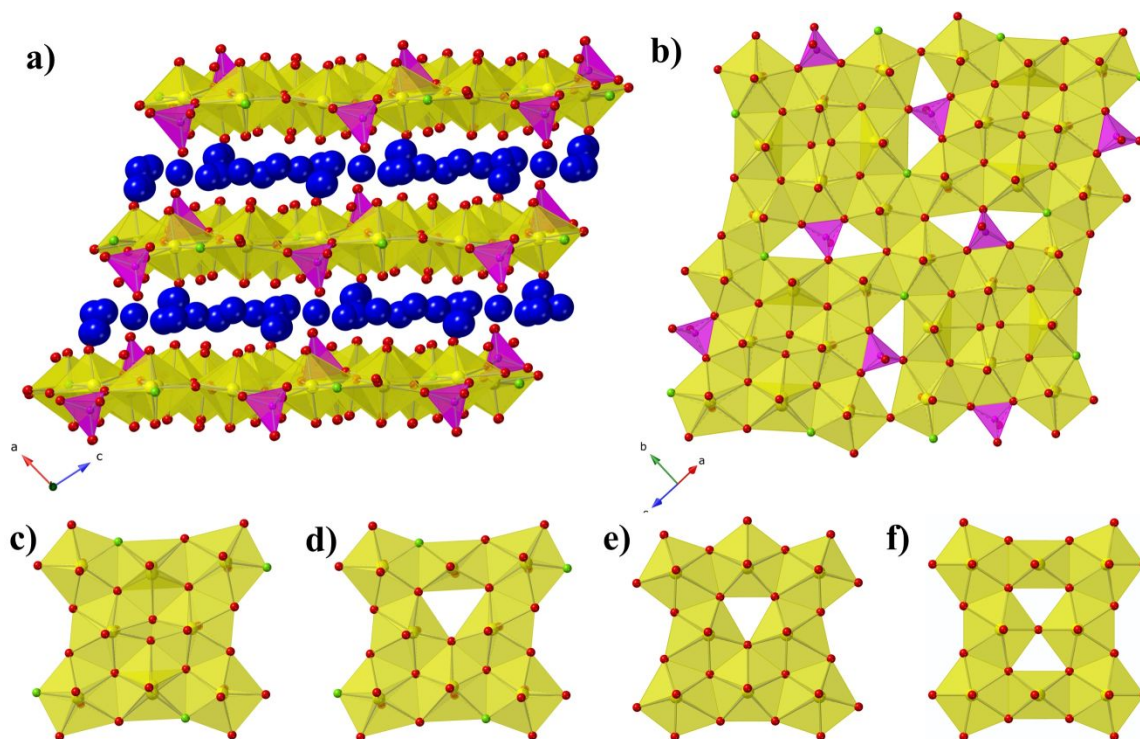trapezoidal gaps in the sheets. These sheets are then stacked with Rb cations residing between the layers.

Figure 7: The layered structure of $Rb_{7.6}[(UO_2)_8O_{8.6}F_{0.4}(PO_4)_2]$ (**5**). a) sheets and Rb cation layers, b) the uranyl phosphate sheets, c) disordered U_3O_8 like, d) idealized U_3O_8 like, e) α-U_3O_8 building, and e) β-U_3O_8 building units.

In other uranyl phosphate oxyfluoride structures,[23] bond valences sums of the anion sites have been useful in identifying the fluorine site, since X-ray diffraction is not always sufficient in determining the location. The bond valence sums[41, 42] for the non-uranyl oxygens range between 1.841 and 2.214 which are in good agreement with the expected value of 2 and do not give any insight as to the location of the fluorine site. The O4 site, which freely refined to an occupancy of ~1.15 in the SXRD structure solution had a bond valence sum value of 1.90. It is important to note that since the occupancy of this site is expected to be 0.80/0.2 O/F based on charge balance, it is not surprising that the small amount of fluorine does not noticeably impact BVS values. In the fluorine doped

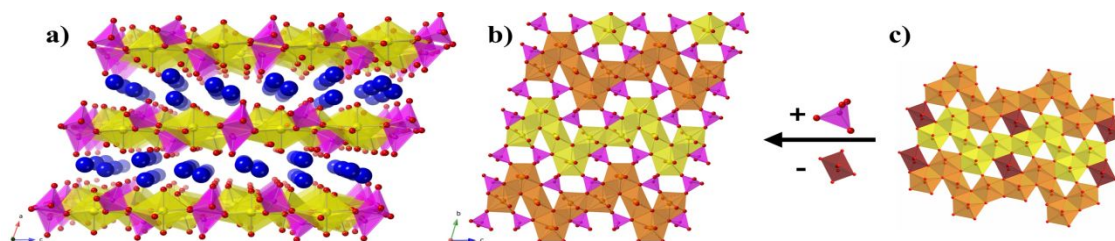phosphuranylite composition the half-occupied fluorine site could not be supported by BVS.[23]

Figure 8: The layered structure of $Rb_6[(UO_2)_5O_2(PO_4)_4]$ (**6**). a) uranyl phosphate sheets and layers of Rb cations, b) the sheet topology of **6**, and c) the sheet topology of β-U_3O_8 and its relation to **6**. Uranium polyhedra are yellow, orange, or red for clarity.

Figure 8c shows the β-U_3O_8 sheets where the chains in $Rb_6[(UO_2)_5O_2(PO_4)_4]$ (**6**) are colored in orange and yellow, and the red uranium polyhedra are the sites removed to obtain the sheet topology in structure **6**. By removing the red uranium polyhedra, separating the yellow and orange chains, and adding phosphate tetrahedra between chains one can obtain the topology of **6** in Figure 8b, which has been previously observed in the As analog synthesized under high-temperature high-pressure methods.[43] These uranyl phosphate sheets stack perpendicular to the *b* direction and the Rb cations reside between the layers.

Several of the structures in this paper, such as **2**, **3**, and **4**, are highly disordered by crystallographic standards, and in order to attempt to quantify the resulting complexity of these structures we have we performed calculations for the total information content of the crystal structures in ToposPro.[44] The procedure as described by Krivovichev was followed and involves calculating the total information of a crystal structure, $I_{G,total}$ (bits/unit-cell) for both the published structure solutions and the idealized solutions where the disorder is removed.[45] For structures where symmetry elements had to be removed in order to simplify the disorder, the total information of the published structure and idealized structure are

reported for the lower symmetry space group (Table 2). Structures **2** and **6** are categorized as intermediate structures, while **3** and **4** are complex and **4** is very complex. By looking at the ratio of $I_{G,total}$ (disordered)/ $I_{G,total}$ (ideal), the complexity of **2**, **3**, and **5** is only mildly increased with the disorder, while the complexity of **4** is nearly doubled as a result of the disorder (ratio of 1.74). [46]

Table 2: Total information content for structures **2-6** (left) and classification (right).[44]

Structure		$I_{G,total}$ (bits/ u.c.)	S. G.
$Cs_2UO_2Ga_2O_5$ (**2**)	Ideal	152	$I4/amd$
	Disordered	242	
$[Rb_2Rb_{3.93}Cl_{0.93}][(UO_2)_5(PO_4)_5]$ (**3**)	Ideal	530	$P\bar{1}$
	Disordered	644	
$Rb_{11}[(UO_2)_8(PO_4)_9]$ (**4**)	Ideal	1854	$Pbam$
	Disordered	3234	
$Rb_{7.6}[(UO_2)_8O_{8.6}F_{0.4}(PO_4)_2]$ (**5**)	Ideal	536	$P2_1$
	Disordered	650	
$Rb_6[(UO_2)_5O_2(PO_4)_4]$		191	$P\bar{1}$

Category	$I_{G,total}$ (bits/ u.c.)
Very simple	< 20
Simple	20-100
Intermediate	100-500
Complex	500-1000
Very complex	>1000

Optical Properties. Fluorescence emission peaks for structures **1-6** lie in the green-yellow region of the visible spectrum which is typical for the uranyl cation (Figure 9). The most intense peaks for structures **1-6** are 528, 533, 529, 524, 533, and 520 nm, respectively and result from the electronic emission from the lowest vibrational level of the first excited state to the lowest vibrational level of the ground state. Smaller peaks around the most intense peak arise from different vibrational levels of the same electronic emission.[47] In the spectra for **1**, **4**, and **6** these vibronic features with defined peak spacing are observed, while in **2**, **3**, and **5** they are not. One explanation is based on the observation that the strength of the uranyl bond affects the spacing between the vibronic features and that stronger bonding decreases the splitting of the emission peaks. [48] To investigate, the average uranyl bond lengths were calculated for structures **2-5** and are 1.848, 1.775, 1.794, 1.815, and 1.807 Å,

respectively. While **2** and **5** have the longest uranyl bonds and fit this previous observation and have essentially no splitting and **1** and **4** have shorter uranyl bond lengths and observable splitting, the shortest bond length, 1.774(10) Å in **3** does not. In previous fluorescence studies, data collected at lower temperatures has been found to significantly increase the resolution of the different vibrational peaks and could help explain the poor peak splitting in **3**. [47]
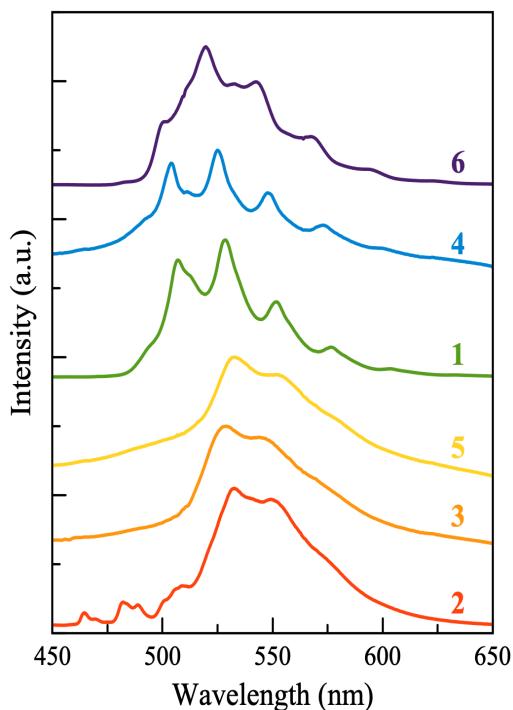

Figure 9: The fluorescence emission spectra of structures **1-6.**

Conclusion. The targeted crystal growth of gallium analogs to the recently published uranium aluminates led to the discovery of a new uranium gallophosphate and a uranium gallate, analogous to previously reported aluminates, in addition to four new uranium phosphates that were obtained within the same phase space. Both the material and

the size/shape of the reaction vessels proved crucial in the isolation of these products, which is somewhat unexpected considering that many publications reporting flux crystal growth neglect to report the size of the crucible used. The phase space explored was not exhaustive, and was explored within reason to target the specific Ga analogs to uranium aluminates and it cannot be concluded whether the Ga analogs of $[Cs_{13}Cl_5][(UO_2)_3Al_2O(PO_4)_6]$, $A_3[Al_2O(PO_4)_3][(UO_2)_3O_2]$ (A = Cs, Rb), and $Rb_7[Al_2O(PO_4)_3][(UO_2)_6O_4(PO_4)_2]$ could not be obtained due to the stability of the other uranium phosphates synthesized from these reactions, or the inability for Ga to replace Al in these structures. While compound **1** could be identified by the powder diffraction and unit cell data, the crystals were not of sufficient quality to obtain a publishable crystal structure, and perhaps different crystal growth methods are necessary to elucidate its structure. Fluorescence spectra for all 6 compositions were obtained and featured typical green-yellow luminescence of the uranyl species.

Supporting Information. The SI contains visual summaries of the UF_4-$GaPO_4$-ACl (A = Cs, Rb) phase space studied in addition to tables of bond valence sums and bond distances U-O, Ga-O, and P-O bonds. CCDC deposition numbers 1984888-1984892 contain the crystallographic data reported in this manuscript.

References:

(1)   Henshaw, D. E., The structure of wadeite, *Mineralogical Magazine and Journal of the Mineralogical Society* **1955**, *30*, 585-595.

(2)   Choisnet, J.; Deschanvres, A.; Raveau, B., Evolution structurale de nouveaux germanates et silicates de type wadeite et de structure apparentee, *J. Solid State Chem.* **1973**, *7*, 408-417.

(3)   Fleet, M. E.; Muthupari, S., Structure of $A_2Ge_4O_9$-Type Sodium Tetragermanate ($Na_2Ge_4O_9$) and Comparison with Other Alkali Germanate and Silicate Mixed Tetrahedral–Octahedral Framework Structures, *J. Solid State Chem.* **1998**, *140*, 175-181.

(4)   Redhammer, G. J.; Tippelt, G., The tetragermanates A2Ge4O9 (A= Na, K and Rb), *Acta Crystallographica Section C: Crystal Structure Communications* **2013**, *69*, 995-1001.

(5)   Morrison, G.; Wilkins, B. O.; Spagnuolo, N. R.; Smith, M. D.; zur Loye, H.-C., Rare earth silicates and germanates crystallizing in the wadeite and related structure types, *J. Solid State Chem.* **2019**, *269*, 51-55.

(6)   Morrison, G.; Kocevski, V.; Misture, S. T.; Spagnuolo, N. R.; Hines, A. T.; Besmann, T.; zur Loye, H.-C., Superwadeites: Elucidation of a Structural Family Related to the Wadeite Structure and Prediction of $Cs_2Ge_5O_{11}$, *Cryst. Growth Des.* **2019**, *19*, 5477-5482.

(7)   Pasero, M.; Kampf, A. R.; Ferraris, C.; Pekov, I. V.; Rakovan, J.; White, T. J., Nomenclature of the apatite supergroup minerals, *Eur. J. Mineral.* **2010**, *22*, 163-179.

(8)   White, T., Apatite - An Adaptive Framework Structure, *Reviews in Mineralogy and Geochemistry* **2005**, *57*, 307-401.

(9)   Grisafe, D. A.; Hummel, F. A., Pentavalent ion substitutions in the apatite structure Part A. Crystal chemistry, *J. Solid State Chem.* **1970**, *2*, 160-166.

(10)   Shaw, D. M., The geochemistry of gallium, indium, thallium—a review, *Physics and Chemistry of the Earth* **1957**, *2*, 164-211.

(11)   Shannon, R. D., Revised effective ionic radii and systematic studies of interatomic distances in halides and chalcogenides, *Acta Cryst.* **1976**, *A32*, 751-767.

(12)   Yu, N.; Klepov, V. V.; Modolo, G.; Bosbach, D.; Suleimanov, E. V.; Gesing, T. M.; Robben, L.; Alekseev, E. V., Morphotropy and Temperature-Driven Polymorphism in A2Th (AsO4) 2 (A= Li, Na, K, Rb, Cs) Series, *Inorg. Chem.* **2014**, *53*, 11231-11241.

(13)   Yin, X.; Wang, Y.; Bai, X.; Wang, Y.; Chen, L.; Xiao, C.; Diwu, J.; Du, S.; Chai, Z.; Albrecht-Schmitt, T. E., Rare earth separations by selective borate crystallization, *Nature communications* **2017**, *8*, 1-8.

(14)   Juillerat, C. A.; Klepov, V. V.; Alekseev, E. V.; zur Loye, H.-C., Overstepping Löwenstein's Rule – a Route to Unique Aluminophosphate Frameworks with 3D Salt-Inclusion and Ion Exchange Properties, *Inorg. Chem.* **2019**, *58*, 724-736.

(15)   Juillerat, C. A.; Kocevski, V.; Besmann, T.; zur Loye, H.-C., Discovery of $Cs_2(UO_2)Al_2O_5$ by Molten Flux Methods: A Uranium Aluminate Containing Solely

Aluminate Tetrahedra as the Secondary Building Unit, *Inorg. Chem.* **2019**, *58*, 4099-4102.

(16) Shvareva, T. Y.; Sullens, T. A.; Shehee, T. C.; Albrecht-Schmitt, T. E., Syntheses, structures, and ion-exchange properties of the three-dimensional framework uranyl gallium phosphates, $Cs_4[(UO_2)_2(GaOH)_2(PO_4)_4] \cdot H_2O$ and $Cs[UO_2Ga(PO_4)_2]$, *Inorg. Chem.* **2005**, *44*, 300-305.

(17) Bugaris, D. E.; zur Loye, H.-C., Materials discovery by flux crystal growth: Quarternary and higher oxides, *Angew. Chem. Int. Ed.* **2012**, *51*, 3780-3811.

(18) Juillerat, C. A.; Klepov, V. V.; Morrison, G.; Pace, K. A.; zur Loye, H.-C., Flux Crystal Growth: A Versatile Technique to Reveal the Crystal Chemistry of Complex Uranium Oxides, *Dalton Trans.* **2019**, *48*, 3162-3181.

(19) Bruker. *APEX3, SAINT+, TWINABS, and SADABS.* Bruker AXS Inc.: Madison, Wisconsin, USA, 2015;

(20) Sheldrick, G. M., Crystal structure refinement with SHELXL, *Acta Cryst.* **2015**, *C71*, 3-8.

(21) Sheldrick, G. M., SHELXT - Integrated space-group and crystal-structure determination, *Acta Cryst.* **2015**, *A71*, 3-8.

(22) Dolomanov, O. V.; Bourhis, L. J.; Gildea, R. J.; Howard, J. A. K.; Pushmann, H., OLEX2: a complete structure solution, refinement and analysis program, *J. Appl. Crystallogr.* **2009**, *42*, 339-341.

(23) Juillerat, C. A.; Kocevski, V.; Besmann, T.; zur Loye, H.-C., Observation of the Same New Sheet Topology in Both the Layered Uranyl Oxide-Phosphate $Cs_{11}[(UO_2)_{12}(PO_4)_3O_{13}]$ and the Layered Uranyl Oxyfluoride-Phosphate $Rb_{11}[UO_2)_{12}(PO_4)_3O_{12}F_2]$ Prepared by Flux Crystal Growth, *Frontiers in Chemistry* **2019**, *7*, 583.

(24) Juillerat, C. A.; Kocevski, V.; Karakalos, S.; Morrison, G.; Misture, S.; Besmann, T.; zur Loye, H.-C., Flux Crystal Growth of U(V) containing oxyfluoride perovskites, *Inorganic Chemsitry Frontiers* **2019**, *6*, 3202-3214.

(25) Juillerat, C. A.; zur Loye, H.-C., Crystal Growth and Structure Characterization of Three Layered Uranyl Phosphates and Their Relation to the Phosphuranylite Family, *Cryst. Growth Des.* **2019**, *19*, 1183-1189.

(26) Juillerat, C. A.; Kocevski, V.; Klepov, V. V.; Amoroso, J. W.; Besmann, T. M.; zur Loye, H.-C., Structure and Stability of Alkali Gallates Structurally Reminiscent of Hollandite, *J. Am. Ceram. Soc. submitted*,

(27) Juillerat, C. A.; Moore, E. E.; Kocevski, V.; Besmann, T. M.; zur Loye, H.-C., A Family of Layered Phosphates Crystallizing in a Rare Geometrical Isomer of the Phosphuranylite Topology: Synthesis, Characterization, and Computational Modeling of $A_4[(UO_2)_3O_2(PO_4)_2]$ (A = alkali metals) Exhibiting Intra-layer Ion Exchange, *Inorg. Chem.* **2018**, *57*, 4726-4738.

(28) Saad, S.; Obbade, S.; Renard, C.; Abraham, F., Synthesis, crystal structure, infrared and electrical conductivity of the layered rubidium uranate $Rb_4U_5O_{17}$, *J. Alloys Compd.* **2007**, *474*, 68-72.

(29) Ling, J.; Wu, S.; Chen, F.; Simonetti, A.; Shafer, J. T.; Albrecht-Schmitt, T. E., Does Iodate Incorporate into Layered Uranyl Phosphates Under Hydrothermal Conditions?, *Inorg. Chem.* **2009**, *48*, 10995-11001.

(30) Juillerat, C. A.; Moore, E. E.; Besmann, T. B.; zur Loye, H.-C., Observation of an Unusual Uranyl Cation-Cation Interaction in the Strongly Fluorescent Layered Uranyl Phosphates $Rb_6[(UO_2)_7O_4(PO_4)_4]$ and $Cs_6[(UO_2)_7O_4(PO_4)_4]$, *Inorg. Chem.* **2018**, *57*, 3675-3678.

(31) Chang, Y.-C.; Chang, W.-J.; Boudin, S.; Lii, K.-H., High-Temperature, High-Pressure Hydrothermal Synthesis and Characterization of a Salt-Inclusion Mixed-Valence Uranium(V,VI) Silicate: $[Na_9F_2][(U^VO_2)(U^{VI}O_2)_2(Si_2O_7)_2]$, *Inorg. Chem.* **2013**, *52*, 7230-7235.

(32) Juillerat, C. A.; Moore, E. E.; Morrison, G.; Smith, M. D.; Besmann, T. M.; zur Loye, H.-C., Versatile Uranyl Germanate Framework Hosting Twelve Different Alkali Halide 1D Salt Inclusions, *Inorg. Chem.* **2018**, *57*, 11606-11615.

(33) Lee, C. S.; Wang, S. L.; Chen, Y. H.; Lii, K. H., Flux synthesis of salt-inclusion uranyl silicates:$[K_3Cs_4F][(UO_2)_3(Si_2O_7)_2]$ and $[NaRb_6F][(UO_2)_3(Si_2O_7)_2]$, *Inorg. Chem.* **2009**, *48*, 8357-8361.

(34) Morrison, G.; Smith, M. D.; zur Loye, H.-C., Understanding the Formation of Salt-Inclusion Phases: An Enhanced Flux Growth Method for the Targeted Synthesis of Salt-Inclusion Cesium Halide Uranyl Silicates, *J. Am. Chem. Soc.* **2016**, *138*, 7121-7129.

(35) Li, H.; Langer, E. M.; Kegler, P.; Modolo, G.; Alekseev, E. V., Formation of Open Framework Uranium Germanates: The Influence of Mixed Molten Flux and Charge Density Dependence in U-Silicate and U-Germanate Families, *Inorg. Chem.* **2018**, *57*, 11201-11216.

(36) Gao, J.; Li, J.; Sulejmanovic, D.; Hwu, S.-J., $M_3(P_2O_7)^{22-}$-Type Open Frameworks Featuring $[M_2O_8]$ and $[M_3O_{12}]$ Multinuclear Transition-Metal Oxide Units. Serendipitous Synthesis of Six Polymorphic Salt-Inclusion Magnetic Solids: $Na_2M_3(P_2O_7)_2 \cdot ACl$ (M = Mn, Fe; A = Rb, Cs) and $K_2M_3(P_2O_7)_2 \cdot CsCl$ (M = Fe, Mn), *Inorg. Chem.* **2015**, *54*, 1136-1144.

(37) Huang, Q.; Hwu, S. J., The fascinating noncentrosymmetric copper (II) phosphates synthesized via CsCl salt-inclusion, *Inorg. Chem.* **2003**, *42*, 665-657.

(38) Hwu, S. J. *A New Class of Hybrid Materials via Salt-inclusion Synthesis.* John Wiley & Sons: 2006; pp 239-250.

(39) West, J. P.; Hwu, S. J., Noncentrosymmetric salt inclusion oxides: Role of salt lattices and counter ions in bulk polarity, *J. Solid State Chem.* **2012**, *195*, 101-107.

(40) Winiarski, M. J.; Tran, T. T.; Chamorro, J. R.; McQueen, T. M., $(CsX)Cu_5O_2(PO_4)_2$ (X = Cl, Br, I): A Family of Cu^{2+} S = 1/2 Compounds with Capped Kagomé Networks COmposed of OCu_4 Units, *Inorg. Chem.* **2019**, *58*, 4328-4336.

(41) Burns, P. C.; Ewing, R. C.; Hawthorne, F. C., The crystal chemistry of hexavalent uranium: polyhedron geometries, bond-valence parameters, and polymerization of polyhedra, *Can. Mineral.* **1997**, *35*, 1551-1570.

(42) Brown, I. D.; Altermatt, D., Bond-valence parameters obtained from a systematic analyses of the inorganic cyrstal structure database, *Acta Cryst.* **1985**, *B41*, 244-247.

(43) Liu, H. K.; Ramachandran, E.; Chen, Y. H.; Chang, W. J.; Lii, K. H., High-Temperature, High-Pressure Hydrothermal Synthesis, Characterization, and Structural Relationships of Layered Uranyl Arsenates, *Inorg. Chem.* **2014**, *53*, 9065-9072.

(44) Blatov, V. A.; Shevchenko, A. P.; Proserpio, D. M., Applied Topological Analysis of Crystal Structures with the Program Package ToposPro, *Cryst. Growth Des.* **2014**, *14*, 3576-3586.
(45) Krivovichev, S. V., Which inorganic structures are the most complex?, *Angewandte Chemie International Edition* **2014**, *53*, 654-661.
(46) Carone, D.; Klepov, V. V.; Smith, M. D.; Zur Loye, H. C., Flux Crystal Growth of Lanthanide Tungsten Oxychlorides, $La_{8.64}W_6O_{30.45}Cl$, $Ce_{8.64}W_{5.74}O_{30}Cl$, and $Ln_{8.33}W_6O_{30}Cl$ (Ln = Pr, Nd): Structural Stability in the Presence of Extreme Cation and Anion Disorder., *Inorg. Chem.* **2019 Dec 16**, *58*, 16831-16837.
(47) Wang, Z.; Zachara, J. M.; Gassman, P. L.; Liu, C.;, O. Q.; Yantasee, W.; Catalano, J. G., Fluorescence spectroscopy of U(VI)-silicates and U(VI)-contaminated Hanford sediment, *Geochim. Cosmochim. Acta* **2005**, *69*, 1391-1403.
(48) Morrison, G.; Tran, T. T.; Halasyamani, P. S.; zur Loye, H.-C., $K_8(K_5F)U_6Si_8O_{40}$: An Intergrowth Uranyl Silicate, *Inorg. Chem.* **2016**, *55*, 3215-3217.